Structure of viscous boundary layers in turbulent Rayleigh-Bénard convection

Ronald du Puits, Christian Resagk, and André Thess
Department of Mechanical Engineering, Ilmenau University of Technology, P.O. Box 100565, 98684 Ilmenau, Germany
(Received 14 April 2009; published 30 September 2009)

Highly resolved profiles of the mean velocity in turbulent Rayleigh-Bénard convection in air are presented and discussed. The present work extends our recently performed experiments at constant aspect ratio [Phys. Rev. Lett. **99**, 234504 (2007)] to variable aspect ratios. The experiments cover a range of Rayleigh numbers $10^9 < \mathrm{Ra} < 10^{12}$ and aspect ratios $1.13 < \Gamma < 11.3$ whereas the Prandtl number is fixed at $\mathrm{Pr}=0.7$. The major finding of the present work is that the profiles of the mean horizontal velocity and its fluctuations are virtually invariant against the variation in Ra or Γ if the wall distance is scaled by the displacement thickness of the boundary layer. Furthermore we have studied typical length scales of the boundary layer and their scaling with Ra and Γ. Regarding a potential transition of the heat transport toward the ultimate regime we found that the boundary layer Reynolds number remains below $\mathrm{Re}_\delta = 250$ which is significantly lower than the predicted limit.

DOI: 10.1103/PhysRevE.80.036318 PACS number(s): 47.27.te, 44.20.+b, 47.50.Ef

I. INTRODUCTION

Although we know at least since Prandtl's experiments in 1932 [1] that the heat transport from a hot (cold) solid surface to a surrounding fluid strongly depends on the flow field near the wall, there is still a substantial lack of knowledge about the velocity field in this convective boundary layer. The Rayleigh-Bénard (RB) system—an adiabatic box in which a fluid is heated from below and cooled from above—is a simple and very well suited model experiment to study this layer. The purpose of the present work is to investigate experimentally the shape of the mean velocity profile near the cooling plate of a large-scale RB system. It is our intention here to evaluate systematically the predictive power of existing phenomenological theories.

The flow in a cylindrical RB cell that we consider here is characterized by three "input parameters," namely, the Rayleigh number $\mathrm{Ra}=(\gamma g \Delta\vartheta H^3)/(\nu\kappa)$, the aspect ratio $\Gamma = D/H$, and the Prandtl number $\mathrm{Pr}=\nu/\kappa$ whereas its response to the applied temperature difference is reflected by the global "output parameters," namely, Reynolds number $\mathrm{Re}=\bar{v}H/\nu$ and Nusselt number $\mathrm{Nu}=(4H\dot{Q})/(\lambda\pi D^2\Delta\vartheta)$. In these definitions the variables stand for the following physical quantities: γ—isobaric expansion coefficient, g—gravitational acceleration, $\Delta\vartheta$—temperature difference between both horizontal plates, ν—kinematic viscosity, κ—thermal diffusivity, D—diameter of the cell, H—plate distance, $\bar{v}$—mean velocity, $\dot{Q}$—convective heat flux, and λ—thermal conductivity.

Because of the absence of experiments meeting both the requirement of high Rayleigh number and high spatial resolution of velocity measurements in recent decades attention has concentrated on the global transfer functions Re (Ra, Pr, Γ) and Nu (Ra, Pr, Γ) (see, e.g., [2–6]). It is beyond any doubt that these functions strongly depend on the structure of the boundary layers near the heated (cooled) wall and theoretical predictions have to imply assumptions regarding the flow field inside these regions. Particularly for high Rayleigh numbers, i.e., $\mathrm{Ra} > 10^{10}$ well-resolved measurements of velocity or temperature are quite scarce. Therefore scaling laws for Re and Nu were often derived on the basis of the assumption that the profile of the mean horizontal velocity is that of an isothermal shear layer over a flat plate. Going that way a number of peculiarities of the convective boundary layer are neglected. This concerns, e.g., the variation in the fluid properties with temperature (see [7]), the superposition and the interaction of both the velocity and the temperature field, the plume advection at the edge of the boundary layer (see [8,9]), and finally the oscillation of the orientation of the outer flow as observed in cylindrical RB cells with aspect ratio $\Gamma \approx 1$ (see [10,11]). There is some evidence that at high Rayleigh numbers $\mathrm{Ra} > 10^7$ (see [12–14]) the temperature does not rise linear with the wall distance as frequently assumed. One might therefore expect that this is also true for the velocity field.

First velocity measurements inside the viscous boundary layer of an air-filled RB experiment were undertaken by Deardorff and Willis [15] and Fitzjarrald [16] using a hot-wire anemometer. However, their measurements were limited to Ra numbers $\mathrm{Ra} < 10^7$ and too small for similarity theories to be applicable. Subsequent velocity measurements inside the boundary layer in highly turbulent RB convection were carried out exclusively in water ($\mathrm{Pr} \approx 5, \ldots, 7$). Applying a photometric dye technique, Belmonte *et al.* [17] found that the mean horizontal velocity in a small cubic water cell rises linear with the distance from the plate. However, the spatial resolution was limited to about six measurement points between the wall and the location of the velocity maximum. The development of laser-based measurement techniques about 15 years ago allowed nonintrusive velocity measurements avoiding any disturbance of the flow. Xia and co-workers [18,19] obtained profiles of the horizontal velocity up to $\mathrm{Ra}=10^{10}$ by measuring the transfer time of particles between two parallel laser beams. Further velocity measurements in water using Particle Image Velocimetry were reported in [20,21] or very recently in [22]. All those experiments confirm the linear rising of the velocity with the plate distance very close to the wall. However, one has to keep in mind that because of the large Prandtl number of water the thermal boundary layer is small compared with the viscous one and it nests within the latter. It clearly differs from $\mathrm{Pr} \approx 1$ fluids where both boundary layers exhibit the same thickness. The present work aims to provide data and to de-

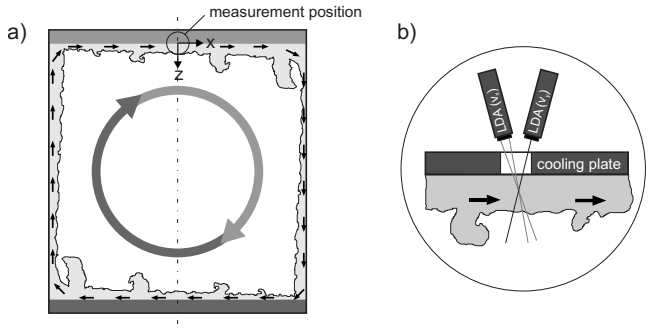

FIG. 1. (a) Sketch of the experimental setup and (b) the 2D laser Doppler anemometer (LDA) velocity measurement along the central axis of the convection cell. The circular arrow in (a) is a schematic representation of the large-scale circulation which occurs for aspect ratios near unity. The light-gray shaded region is a qualitative sketch of the velocity boundary layers (not to scale).

rive scaling relations for those fluids which are relevant for many natural and technical processes. For that purpose we use a large-scale RB experiment which has been operated by our group since the year 2001. In this experimental facility—also called the "Barrel of Ilmenau"—we study the velocity field up to $\mathrm{Ra}=10^{12}$ by using a two-dimensional (2D) Laser Doppler anemometer (LDA).

The outline of the paper is as follows. In Sec. II we describe the experimental facility, the measurement setup, and the data processing algorithms. In Secs. III and IV the results at constant and variable aspect ratio, respectively, are discussed and our intention is to answer particularly the following three questions:

(i) Does the model of an isothermal shear flow over a flat plate adequately describe the mean flow profile of the convective boundary layer?

(ii) How does the structure of the velocity field inside the boundary layer depend on the Rayleigh number and on the aspect ratio?

(iii) How do typical length scales depend on the Rayleigh number and on the aspect ratio?

In Sec. V the results are summarized. A brief account of a limited part of this work, namely, the mean velocity profiles for $\Gamma \approx 1$, has been given in [23].

II. EXPERIMENTAL SETUP

The data presented here were all obtained in a cylindrical RB cell 7.15 m in diameter which is sketched in Fig. 1(a). The cell confines ambient air whose Prandtl number of $\mathrm{Pr}=0.7$ is nearly constant over the temperature range investigated here. An electrical heating plate at the bottom as well as a free-hanging cooling plate at the top trigger the convective motion of the flow. The distance between both plates can be varied continuously from $H=0.05$ m up to a maximum possible value of $H=6.30$ m. Between both plates a temperature difference $4\ \mathrm{K}<\Delta\vartheta<60$ K can be applied. The variation in both quantities H and $\Delta\vartheta$ corresponds to a very wide range of input parameters, namely, $10^5<\mathrm{Ra}<10^{12}$ and $1.13<\Gamma<150$. However, in the present work we focus on Rayleigh numbers $\mathrm{Ra}>7\times10^8$ and aspect ratios $1.1<\Gamma<11.3$. The nonuniformity of the temperature over the surface of the cooling plate is typically less than 0.3 K at the lower bound of $\Delta\vartheta$ and less than 1.0 K at the upper one. Both plates are leveled horizontally with a maximum error of 0.1° and their distance is measured with an accuracy better than 1 cm. In order to ensure the adiabatic boundary condition the sidewall of the cell consists of two insulating layers with an electrical panel heating system in between. The temperature of each of the 18 heating panels around the cell is controlled in such a way that the temperature of the panel is equal to the temperature at the interface between the inner insulating layer and the air. As long as the temperature inside the RB cell does not fall below the ambient temperature—a condition which was satisfied in all experiments reported here—this system effectively prevents the heat flow through the sidewall. A more detailed description of the apparatus is given in one of our previous papers [13].

The present work is exclusively concerned with measurements of profiles of the mean horizontal velocity and its fluctuations. All profiles were measured along the central axis near the cooling plate, as shown in Fig. 1(b). A glass window with a diameter of 8 cm permitted the optical access for the LDA. Since it is known from previous works that the orientation of the horizontal velocity vector in cylindrical RB cells varies over a wide angle (see, e.g., [24,25]), a simple one-dimensional measurement of the velocity was found to be insufficient to provide reliable velocity profiles. In order to demonstrate this, Fig. 2(a) shows how strongly the direction of the large-scale circulation changes over large time scales. More precisely, it shows the mean angle $\phi(z)$ of the horizontal velocity vector (to be defined below) for the full 48 h profile measurement at $\Gamma=1.13$ and $\mathrm{Ra}=5.38\times10^{11}$. Each of the points corresponds to the time average over a 1 h series at a fixed distance z from the cooling plate. Since z has been increased by one step per hour, the profile shown in Fig. 2(a) can be considered as the time history of the orientation of the large-scale circulation. Unlike in rectangular or slightly tilted cylindrical RB cells where the mean flow is forced into a fixed direction (see, e.g., [26]), this shows that in our experiment the mean angle of the flow undergoes variations as large as about $\pi/4$ (e.g., +29° at $z=85$ mm and −16° at $z=90$ mm). Therefore it was found necessary to simultaneously measure both horizontal velocity components using two single LDA probes with different orientation.

The probes were mounted on a high precision traverse system with a mutual angle of $\varphi=21°$ and could be moved in vertical (z) direction in steps of $\Delta z=0.01$ mm. They were adjusted to ensure that the measurement volumes coincide in the same point of space. The position $z=0$ mm was defined as the point at which the centers of the measurement volumes (which are ellipsoids with a diameter of about 0.1 mm and a length of about 1.5 mm) were located precisely at the lower surface of the glass window. The fact, that a fraction of the measurement volume penetrates the glass window for all positions $z<0.75$ mm, causes a small positive measurement error, and distorts the near-wall parts of the profiles discussed in Secs. III and IV. For all LDA measurements cold-atomized droplets of Di-Ethyl-Hexyl-Sebacat (DEHS) with a size of about 1 μm were used as tracer particles. They were injected at the edge of the cooling plate far from the mean flow during a short time of approximately 15 s/h.

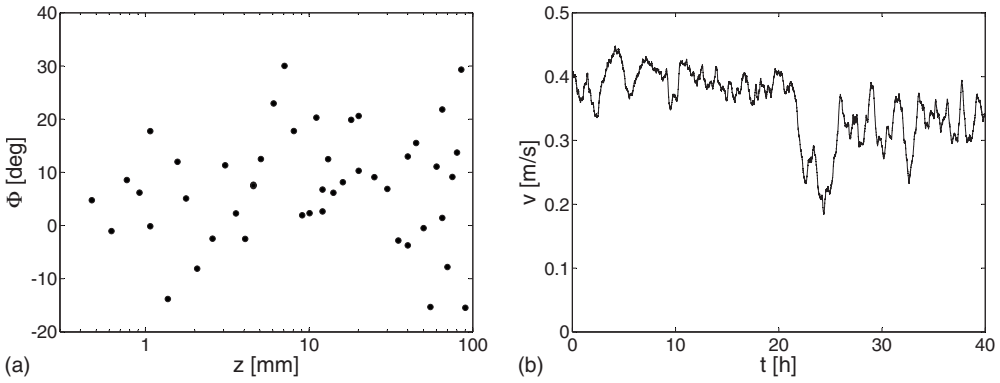

FIG. 2. Particular properties of the velocity vector measured at the central axis of a cylindrical RB experiment near the cooling plate: (a) mean angle ϕ of the velocity vector over the profile measurement at $\Gamma=1.13$ and $\mathrm{Ra}=5.38\times10^{11}$, each point corresponds to a time series of 1 h at a fixed distance z and (b) moving average of the horizontal velocity measured with an omnidirectional hot-film sensor at $\Gamma=1.13$ and $\mathrm{Ra}=7.15\times10^{11}$.

Time series of both horizontal velocity components $v_x(z,t)$ and $v_y(z,t)$ were captured at 39 different z positions starting at $z=90$ mm and up to the smallest distance from the plate $z=0.47$ mm. We are mainly interested in the mean velocity and its fluctuations. In order to obtain reliable data free from statistical errors it is required that the length of the time series significantly exceeds the longest time scales of the velocity signal. In Fig. 2(b) a typical turbulent velocity signal measured at $z=150$ mm using an omnidirectional hot-film sensor at $\Gamma=1.13$ and $\mathrm{Ra}=7.15\times10^{11}$ is plotted. The sampling rate of the measurement was 0.1 s^{-1}, but the graph presents the moving average over a period of 360 s. The example shows that the largest time scales of the evolution of the horizontal velocity are at least of the order of 5 h, i.e., 450 times larger than an eddy turnover time of the large-scale circulation which is about 40 s. Occasional events such as the velocity breakdown between the hours 21 and 26 where the magnitude of the horizontal velocity decreased by about a 40% reduce the quality of the statistics of the data again. Due to this fact time series of at least 50 h at each position z would be required to produce data with high statistical accuracy but it was impossible to realize in our present setup. So we decided to limit the measurement time to 1 h at each position keeping in mind that the results are slightly more uncertain than, e.g., those obtained in isothermal shear flows.

Before we started with the data processing, all time series had to run a prefiltering process in which spurious bursts from the surface of the glass window and readings outside a limit of five standard deviations around the mean were removed. In the next step the data stochastically sampled and prefiltered were transformed into equidistant time series $v_x'(z,t)$ and $v_y'(z,t)$ and the magnitude $v(z,t)=[v_x'^2(z,t)+v_y'^2(z,t)]^{1/2}$ as well as the relative angle $\phi(z,t)=\arctan[v_y'(z,t)/v_x'(z,t)]$ against the arbitrarily defined x axis was computed as functions of time. The composition of the mean values $\bar{v}(z)$ of each of those time series yielded the profile of the mean horizontal velocity which is the central focus of our work. Their errors were estimated as the 95% confidence interval around the mean $\bar{v}(z)\pm2\sigma/\sqrt{N}$, where σ and N are the standard deviation and the number of stochastically independent values in each time series.

Unlike in the usually used definition of the Rayleigh number we substituted $\Delta\vartheta$ by twice the difference between the measured bulk temperature and the very homogeneous temperature of the cooling plate $\Delta\vartheta=2(\bar{\vartheta}_B-\bar{\vartheta}_{CP})$. This avoids uncertainties coming from the nonuniformity of the bottom plate temperature. All quantities appearing in the similarity parameters were evaluated for the bulk temperature $\bar{\vartheta}_B$.

III. RESULTS FOR CONSTANT ASPECT RATIO

We start our discussion by presenting the profiles of the mean horizontal velocity at constant aspect ratio $\Gamma=1.13$. As reported in numerous experimental and numerical works by, e.g., Verzicco and Camussi [27], Sreenivasan *et al.* [28], or Xia *et al.* [26] the convective flow develops a very stable single roll in RB cells of a cylindrical geometry with aspect ratio of order unity. This roll almost fills the space of the cell and forms distinct velocity boundary layers at both horizontal plates. However, there is as yet little consensus about the detailed structure of the flow field inside those layers particularly at high Rayleigh numbers $\mathrm{Ra}>10^{10}$. Since, however, it is a widely held view that the boundary layer remains laminar up to at least $\mathrm{Ra}=10^{14}$ (see, e.g., [4]) we first inquire whether our profiles can be approximately described by that of a laminar shear layer of Blasius type.

To this end we have plotted the measured profiles in a normalized form as $v^*(\eta)$ with $v^*=\bar{v}/\bar{v}_{max}$ and $\eta=z\sqrt{\bar{v}_{max}/2\nu x}$ (see Fig. 3). Guided by the hypothesis that the velocity boundary layer starts to evolve at the sidewall and arrives at the center of the cooling plate after having traversed a path of approximately $D/2=3.5$ m, we have initially attempted to use $x=D/2$ to define η. With this choice of the evolution length scale the velocity profiles were found to diverge significantly from the Blasius solution. This observation indicates that the picture of a horizontally evolving laminar boundary layer may not be correct for the range of parameters considered here. Instead of this first approach we then adjusted the free parameter x to have the same slope $\partial v^*/\partial\eta|_{\eta=0}$ at the wall as the Blasius profile. A selection of

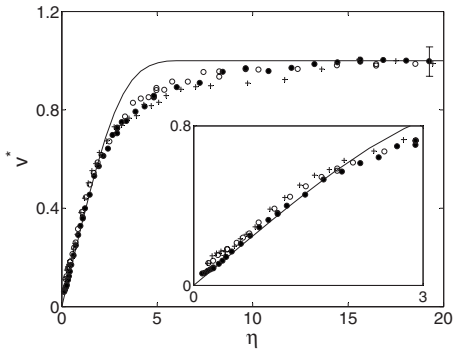

FIG. 3. Profiles of the mean velocity at constant aspect ratio $\Gamma=1.13$ for three different Rayleigh numbers $\mathrm{Ra}=1.23\times10^{11}$ (full circles), $\mathrm{Ra}=5.38\times10^{11}$ (empty circles), and $\mathrm{Ra}=9.77\times10^{11}$ (crosses) compared with the Blasius solution $v^*(\eta)$ (solid line). The inset shows the nearly linear behavior of the profiles close to the surface of the cooling plate.

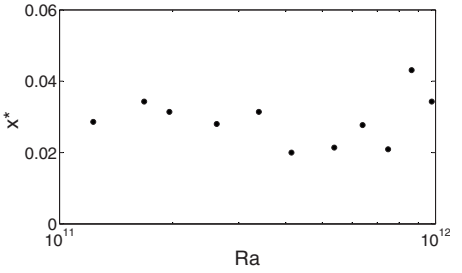

FIG. 4. Length scale $x^*=2x/D$ to match the near-wall gradients of the measured velocity profiles with that of the Blasius solution and its dependency on Ra.

data along with the mean velocity profile according to Blasius is shown in Fig. 3. It is worth pointing out that the length scale x (see Fig. 4 and Table I) was only of the order of $x\approx10$ cm and about 30 times less than the natural path length $D/2$ along the plate. The quantity remained virtually unchanged in the parameter range of Ra investigated here. This is a further indication that the near-wall region in turbulent convection exhibits a different evolution than we know from typical boundary layers, e.g., in aerodynamics.

Due to our adjustment regarding $\partial v^*/\partial\eta|_{\eta=0}$ all measured profiles almost coincide with the linear part of the Blasius solution for $\eta<2$. Small deviations from the linear shape are caused by the systematic error of the measurements very close to the wall and in the definition of the position $z=0$ mm (see the inset of Fig. 3). Following the shape of the normalized profiles toward larger distances all profiles collapse again for $\eta>15$ but they are noticeably lower than the prediction of the laminar shear layer in the intermediate range $2<\eta<15$. The highest deviation is at $\eta\approx5$, usually considered as the edge of the laminar boundary layer. In a convective boundary layer this region is characterized by the permanent advection of plumes interacting with the mean (outer) flow. It is clear that these plumes generate an additional wall-normal flow component which strongly enhances the momentum transport leading to the larger flatness of velocity profiles in convective boundary layers. A better understanding of these processes will be possible once we know the wall-normal velocity component v_z. However, this was not measurable in the current setup and will be part of our future work.

As known long time ago the heat transfer through a RB cell also depends on the relation between the thermal and the viscous boundary layer (see, e.g., [17]). In a gas like air with nearly the same coefficients ν and κ for molecular momentum and heat transport, one expects that velocity and temperature rise in the same manner with increasing distance from the cooling plate. Indeed, if we scale both quantities such that $v^*,\Theta^*=0$ at the surface of the plate and $v^*,\Theta^*=1$ at their maximum, both profiles are quite similar in spite of the fact that there is no direct correspondence between velocity and temperature. One typical example of this similarity is plotted in Fig. 5 at $\mathrm{Ra}\approx4\times10^{11}$ but this agreement can

TABLE I. Set of parameters and selected results for the constant aspect ratio $\Gamma=1.13$, $\mathrm{Pr}=0.7$ measurement series. Ra_v and Ra_Θ are the Rayleigh numbers adjusted during the velocity and the temperature measurements, respectively, x is the path length used for the computation of η, δ_v and δ_Θ are the displacement thicknesses for the viscous and the thermal boundary layer, $\bar{v}_{max}$ is the maximum of the velocity, and Re_δ is the boundary layer Reynolds number.

Ra_v (10^{11})	x (m)	δ_v (mm)	$\bar{v}_{max}$ (m/s)	Re_δ	Ra_Θ (10^{11})	δ_Θ (mm)
1.23	0.100	11.35	0.179	133	1.08	12.68
1.68	0.120	8.12	0.212	112	1.42	11.06
1.98	0.110	8.66	0.220	124	1.86	0.39
2.62	0.098	6.99	0.262	118	2.54	9.87
3.39	0.110	6.97	0.301	134	3.34	9.03
4.14	0.070	7.61	0.339	162	4.19	7.86
5.38	0.075	5.95	0.404	149	5.42	7.84
6.40	0.097	4.87	0.435	129	6.37	7.53
7.48	0.073	6.52	0.503	195	7.76	6.77
8.64	0.151	5.28	0.545	167	8.59	6.96
9.77	0.120	7.27	0.607	251	9.78	6.73

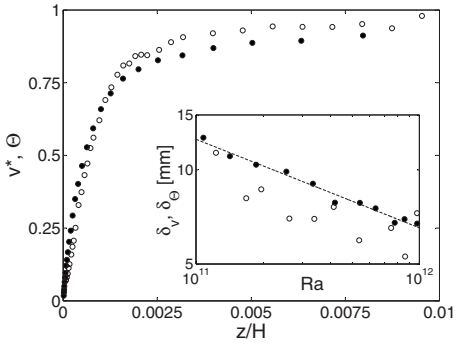

FIG. 5. Viscous and thermal boundary layer at constant aspect ratio $\Gamma=1.13$: mean profiles of the normalized velocity v^* (empty circles) and the normalized temperature Θ (full circles) for $\mathrm{Ra}\approx 4\times 10^{11}$. The inset shows the displacement thickness of the viscous (empty circles) and the thermal boundary layer (full circles) depending on the Rayleigh number. The dotted line corresponds to a power law $\delta\sim \mathrm{Ra}^{-0.25}$.

be found for $\Gamma=1.13$ and all Rayleigh numbers investigated in this work.

In order to compare the profiles of velocity and temperature quantitatively we computed the thicknesses of the viscous and the thermal boundary layer. Unlike in previous works (see, e.g., [17]) in which the authors computed these quantities from the near-wall gradient of the velocity and the temperature profile, our highly resolved profiles enable us to determine the displacement thickness which is a more global quantity and which better describes the full shape of the profiles. It is usually defined as

$$\delta_v = \int_0^\infty \left\{1 - \frac{\bar{v}(z)}{\bar{v}_{max}}\right\} dz, \tag{1}$$

$$\delta_\Theta = \int_0^\infty \left\{1 - \frac{\bar{\vartheta}'(z)}{\bar{\vartheta}_{max}}\right\} dz, \tag{2}$$

where $\bar{\vartheta}'=\bar{\vartheta}(z)-\bar{\vartheta}_{CP}$ is the difference between the measured temperature and the surface temperature of the cooling plate (see, e.g., [29]). In the following it will referred to as defect temperature. We computed δ_v and δ_Θ by a discrete summation over the profiles according to the following equations:

$$\delta_v = z_{v,max} - \frac{1}{\bar{v}_{max}} \sum_{i=1}^{K-1} \frac{1}{2}(\bar{v}_{i+1}+\bar{v}_i)(z_{i+1}-z_i), \tag{3}$$

$$\delta_\Theta = z_{\Theta,max} - \frac{1}{\bar{\vartheta}'_{max}} \sum_{i=1}^{K-1} \frac{1}{2}(\bar{\vartheta}'_{i+1}+\bar{\vartheta}'_i)(z_{i+1}-z_i). \tag{4}$$

The inset of Fig. 5 shows the results compared with the theoretical prediction $\delta_v\sim \mathrm{Ra}^{-0.25}$ from [4]. However, due to the limited domain of Ra of just one order of magnitude and the statistical scatter of the results we do not trust to judge about any differences between both scalings.

An open question of fundamental importance in RB convection is the existence of the so-called "ultimate regime," an enhancement of the heat transfer caused by the transition

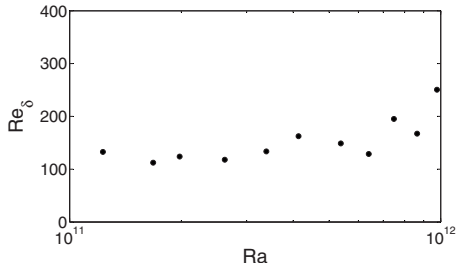

FIG. 6. Boundary layer Reynolds number $\mathrm{Re}_\delta=\bar{v}_{max}\delta_v/\nu$ depending on the Rayleigh number.

of the boundary layer from the laminar to the turbulent state. First it has been predicted by Kraichnan [30] at $\mathrm{Ra}\approx 10^{18}$. In a refined theoretical analysis Grossmann and Lohse lowered that limit to $\mathrm{Ra}\approx 10^{14}$ [31] for gases with $\mathrm{Pr}\approx 0.7$. However, a clear experimental evaluation of this hypothesis is still missing. There is as well an experiment showing an enhancement in the heat transfer below $\mathrm{Ra}=10^{12}$ [32] as there are facilities in which the scaling exponent remains unchanged until $\mathrm{Ra}=10^{17}$ [5] and $\mathrm{Ra}=3\times 10^{14}$ [33]. Our velocity measurements enable us to evaluate directly the boundary layer Reynolds number which is defined as

$$\mathrm{Re}_\delta = \bar{v}_{max}\delta_v/\nu. \tag{5}$$

This quantity is an appropriate criterion to find a signature for a potential transition to a turbulent boundary layer. Based on a stability analysis Schlichting and Gersten estimated this bound for an isothermal shear layer over a flat plate to $\mathrm{Re}_{\delta,c}=520$ [29]. Under the influence of an additional temperature gradient across the boundary layer Preston [34] as well as Grossmann and Lohse [4] predicted values of $\mathrm{Re}_{\delta,c}=320$ and $\mathrm{Re}_{\delta,c}=420$, respectively. We plot our values of Re_δ in the domain $10^{11}<\mathrm{Ra}<10^{12}$ in Fig. 6. Below $\mathrm{Ra}=6\times 10^{11}$ the boundary layer Reynolds number remains roughly constant at $\mathrm{Re}_\delta\approx 120$, significantly below the lowest prediction limit predicted. Above this bound it slightly increases, but in the range of Ra investigated here it never exceeds the lowest critical value of $\mathrm{Re}_{\delta,c}=320$. However, extrapolating the graph into the next decade of Ra, the limit will be exceeded and the boundary layer might become turbulent. Neither from the boundary layer Reynolds number nor from the shape of the velocity or the temperature profiles a transition to a turbulent boundary layer is indicated up to at least $\mathrm{Ra}=10^{12}$. This finding agrees well with Grossmann's prediction derived from the scaling theory [31] and also with very recent measurements in compressed sulfur hexafluoride ($\mathrm{Pr}\approx 0.8$) by Funfschilling *et al.* [33] where a transition in the global heat flux was not observed up to $\mathrm{Ra}=3\times 10^{14}$.

Having discussed the profiles of the mean velocity we now turn to the profiles of the fluctuations $v_{rms}(z)=\sigma_v(z)/v_{max}$, where σ_v stands for the standard deviation (in m/s) of the time series $v(z,t)$. Whereas a number of predictions exist for the profiles of the vertical velocity fluctuations, such as $\sigma_{vz}\sim z^{1/3}$ (see [35]) and $\sigma_{vz}\sim \ln z$ predicted by Adrian *et al.* [36] and experimentally verified by Fernandes and Adrian [20], our knowledge about fluctuations of the horizontal velocity is rather limited. Solely Xin and Xia mea-

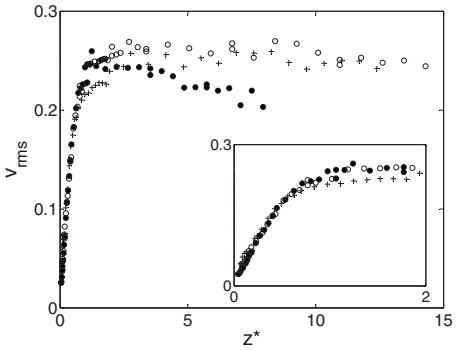

FIG. 7. Profiles of the fluctuations of the horizontal velocity at constant aspect ratio $\Gamma=1.13$ for three different Rayleigh numbers $\mathrm{Ra}=1.23\times10^{11}$ (full circles), $\mathrm{Ra}=5.38\times10^{11}$ (empty circles), and $\mathrm{Ra}=9.77\times10^{11}$ (crosses).

sured the fluctuations of one horizontal velocity component in a water filled RB experiment at $\mathrm{Pr}\approx7$ [37]. For $\mathrm{Ra}<10^{11}$ they found out that $\sigma_{vx}\sim z$ but the spatial resolution of their measurements was not sufficient to differentiate between various predictions. We plot three examples of the two-dimensional horizontal velocity fluctuations at $\mathrm{Ra}=1.23\times10^{11}$, $\mathrm{Ra}=5.38\times10^{11}$, and $\mathrm{Ra}=9.77\times10^{11}$ in Fig. 7. All profiles were normalized by the boundary layer thickness δ_v. Below their maximum at $z\approx\delta$ the profiles collapse very well (see inset). Corresponding to the observation of Xin and Xia they rise linearly with the plate distance z irrespective of the systematic measurement error very close to the wall. An interesting observation is that for $\mathrm{Ra}=1.23\times10^{11}$ the fluctuations decay after reaching a maximum while they remain approximately constant for the other ones. However, we do not want to judge here whether this phenomenon is physically justified or it is simply generated by the statistical uncertainties of the measurements.

IV. RESULTS FOR VARIABLE ASPECT RATIO

In the second part of our work we discuss the influence of the aspect ratio on the velocity field inside the boundary layer at the cooling plate. It would have been desirable to investigate the properties of the viscous boundary layer while varying the aspect ratio only and keeping the Rayleigh number constant. In our experiment, however, this would require to change the temperature difference by a factor of 1000 in order to compensate for the tenfold decrease in the height, necessary to increase the aspect ratio from 1.13 to 11.3. Since this is impossible, our variation in the aspect ratio is accompanied by a simultaneous variation in the Rayleigh number.

While for $\Gamma\approx1$ and sufficiently large Rayleigh numbers one single roll develops inside cylindrical RB cells, this roll is replaced by multiple structures at higher aspect ratios (see, e.g., [25,38]). Supposing that the flow field inside the boundary layer is affected by the global flow structure we expected the mean velocity field inside the boundary layer to be variable with changing Γ. In order to evaluate this hypothesis a second series of experiments was undertaken in which the temperature difference between the heating and the cooling plates was maintained at $\Delta\vartheta=40$ K and the aspect ratio was varied between its lowest possible value $\Gamma=1.13$ (corresponding to $\mathrm{Ra}=7.48\times10^{11}$) and $\Gamma=11.3$ ($\mathrm{Ra}=7.16\times10^{8}$). The exact parameters and the results can be found in Table II.

At first we discuss the profiles of the mean horizontal velocity. Three examples at $\Gamma=1.13$, $\Gamma=2.45$, and $\Gamma=6.81$ are shown in normalized form $v^*(z^*)=\bar{v}(z^*)/\bar{v}_{max}$ over $z^*=z/\delta_v$ in Fig. 8. Despite the not insignificant statistical scatter of the data points the profiles remain virtually universal. This result obtained under the influence of various global flow structures is quite surprising for the moment but it supports the hypothesis that the developing of the convective boundary layer differs from that of an isothermal shear layer evolving along a flat plate.

As already discussed in Sec. III the ratio of the thicknesses of the viscous and the thermal boundary layer δ_v and δ_Θ is of interest because some phenomenological scaling theories describing the global momentum and heat transport in turbulent RB convection (see, e.g., [4]) rest upon assump-

TABLE II. Set of parameters and selected results for the variable aspect ratio measurement series at constant temperature difference $\Delta\vartheta=40$ K. Ra_v and Ra_Θ are the Rayleigh numbers adjusted during the velocity and the temperature measurements, respectively, δ_v and δ_Θ are the displacement thicknesses for the viscous and the thermal boundary layer, $\bar{v}_{max}$ is the maximum of the velocity, and Re_δ is the boundary layer Reynolds number.

Γ	Ra_v	δ_v (mm)	$\bar{v}_{max}$ (m/s)	Re_δ	Ra_Θ	δ_Θ (mm)
11.3	7.16×10^{8}	2.10	0.168	21	8.14×10^{8}	4.67
8.83	1.51×10^{9}	2.38	0.174	25	1.67×10^{9}	5.23
6.81	3.37×10^{9}	3.33	0.185	37	3.54×10^{9}	5.66
5.26	7.43×10^{9}	4.06	0.213	51	7.56×10^{9}	6.06
4.06	1.62×10^{10}	4.29	0.236	60	1.66×10^{10}	6.16
3.15	3.46×10^{10}	5.08	0.325	98	3.53×10^{10}	6.42
2.45	7.42×10^{10}	5.02	0.378	113	7.66×10^{10}	6.65
1.89	1.62×10^{11}	4.97	0.438	130	1.69×10^{11}	7.00
1.47	3.47×10^{11}	5.66	0.590	199	3.66×10^{11}	7.56
1.13	7.48×10^{11}	6.51	0.503	195	7.70×10^{11}	6.77

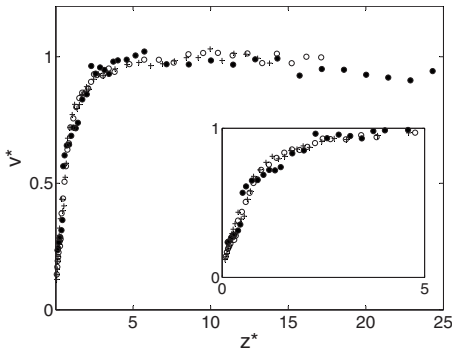

FIG. 8. Profiles of the mean velocity for different aspect ratios $\Gamma=1.13$ (crosses), $\Gamma=2.45$ (empty circles), and $\Gamma=6.81$ (full circles). The inset shows the region very close to the wall.

tions about it. We plot both quantities as a function of the aspect ratio in Fig. 9. As seen in Sec. III the thicknesses of both boundary layers roughly correspond for the case of $\Gamma=1.13$. However, with increasing aspect ratio the viscous boundary layer shrinks faster than the thermal one does. Using a least squares fit these experimental observations can be approximately described by the relations

$$\delta_v(\Gamma) = 6.873^{\pm 0.362}\ \text{mm} \times \Gamma^{-0.3899 \pm 0.0477} \tag{6}$$

and

$$\delta_\Theta(\Gamma) = 7.604^{\pm 0.245}\ \text{mm} \times \Gamma^{-0.1632 \pm 0.0245}, \tag{7}$$

indicating that with decreasing distance between both horizontal plates the momentum transport throughout the boundary layer becomes more effective than the heat transport. A very interesting aspect would be to compensate the obtained relations $\delta_v(\Gamma)$ and $\delta_\Theta(\Gamma)$ (which also include as a matter of fact a dependency on Ra by the Rayleigh dependency from the constant aspect ratio measurements, but unfortunately the latter one is not well defined and so we renounced here to do it).

Using the obtained values of δ_v we compute a boundary layer Reynolds number and plot the results in Fig. 10. It is not a surprise that with rising aspect ratio Re_δ drops to values of the order $\mathrm{Re}_\delta \approx 20$ far away from the transition limit to the turbulent boundary layer.

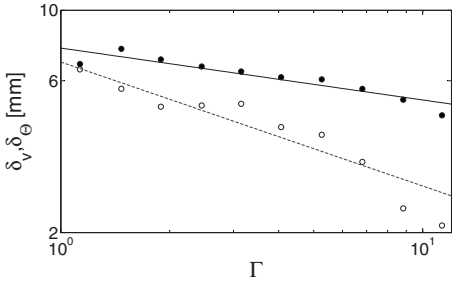

FIG. 9. Thickness of the viscous (empty circles) and the thermal (full circles) boundary layer over the aspect ratio for constant temperature difference $\Delta\vartheta=40$ K. The dashed line corresponds to a power law $\delta_v=6.873\ \text{mm}\times\Gamma^{-0.3899}$; the full line corresponds to $\delta_\Theta=7.604\ \text{mm}\times\Gamma^{-0.1632}$.

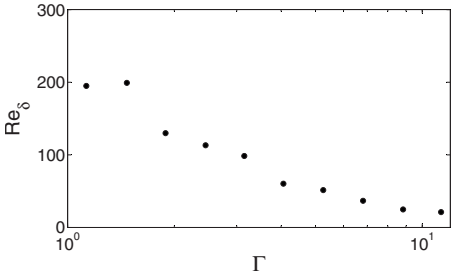

FIG. 10. Boundary layer Reynolds number $\mathrm{Re}_\delta = v_{max}\delta_v/\nu$ over the aspect ratio for a fixed temperature difference $\Delta\vartheta=40$ K.

Finally we analyze the profiles of the horizontal velocity fluctuations and how they depend on Γ. From the constant aspect ratio experiments we know that neither the shape of the profiles nor their maxima depend on the temperature difference between the heating and the cooling plates. We plot three selected examples of $v_{rms}(z^*)$ in Fig. 11. Using the boundary layer thickness to scale the distance from the surface of the plate we find that all profiles are virtually invariant against a variation in Γ at least inside the boundary layer. Outside this near-wall region where the plumes intensively interact with the global flow the fluctuations reach a maximum. Its value increases with increasing aspect ratio. A serious hypothesis to explain this observation would require additional information about the fluctuations of the wall-normal velocity component and a detailed knowledge about the global flow structure at aspect ratios larger than $\Gamma=1$ which are not available until now.

V. CONCLUSIONS

The major finding of the present work is that the profiles of the mean horizontal velocity and its fluctuations are invariant against the variation in Ra or Γ if the wall distance is scaled by the displacement thickness of the boundary layer. In a parameter domain $10^9<\mathrm{Ra}<10^{12}$ and $1.13<\Gamma<11.3$ none of the measured profiles were found to match the Blasius profile for the laminar flow in an isothermal shear layer over a flat plate. Particularly in the outer region of the boundary layer the velocity gradient $\partial\bar{v}/\partial z$ was smaller than

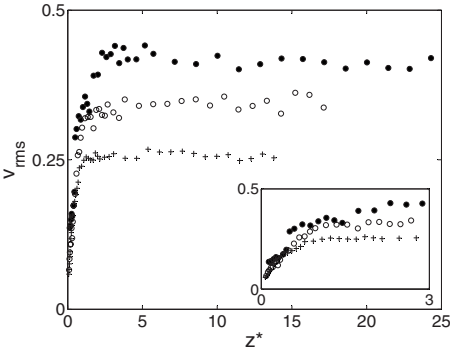

FIG. 11. Profiles of the horizontal velocity fluctuations for different aspect ratios $\Gamma=1.13$ (crosses), $\Gamma=2.45$ (empty circles), and $\Gamma=6.81$ (full circles). The inset shows the profiles in the near-wall region $z^*<3$ in linear scaling.

expected from the prediction of a laminar shear flow. This finding indicates that the wall-normal momentum transport in a convective boundary layer is higher than in a laminar shear flow of constant temperature. One hypothesis to explain it might be the formation of thermal plumes inside the boundary layer and their interaction with the outer flow. However, in order to fully understand this process measurements of the wall-normal velocity component are required. The fluctuations of the horizontal velocity rise linearly with the plate distance z inside the boundary layer. They reach their maximum at $z \approx \delta$ but the value of these maxima depends on the aspect ratio.

For a fixed aspect ratio of about unity viscous and thermal boundary layer exhibit roughly the same thickness and they scale with the Rayleigh number in a similar manner (irrespective the parameter range outside the Boussinesq approximation). With increasing aspect ratio, the viscous boundary layer shrinks faster than the thermal one does corresponding to power laws $\delta_v = 6.873\ \text{mm} \times \Gamma^{-0.3899}$ and $\delta_\Theta = 7.604\ \text{mm} \times \Gamma^{-0.1632}$, respectively. In all cases the boundary layer Reynolds number Re_δ derived from those values of δ_v remains below $\text{Re}_\delta = 250$ indicating that the boundary layer does not become turbulent up to $\text{Ra} = 10^{12}$.

ACKNOWLEDGMENTS

The authors wish to acknowledge the financial support of the Deutsche Forschungsgemeinschaft under Grant No. Th 497 and of the Thüringer Ministerium für Wissenschaft, Forschung und Kunst for the work reported in this paper. Furthermore, we thank J. Schumacher for stimulating discussions as well as V. Mitschunas, K. Henschel, H. Hoppe, and T. Ryll for their technical assistance.

[1] L. Prandtl, Beitr. Phys. Atmos. **19**, 188 (1932).
[2] B. Castaing *et al.*, J. Fluid Mech. **204**, 1 (1989).
[3] E.-D. Siggia, Annu. Rev. Fluid Mech. **26**, 137 (1994).
[4] S. Grossmann and D. Lohse, J. Fluid Mech. **407**, 27 (2000).
[5] J.-J. Niemela and K.-R. Sreenivasan, J. Fluid Mech. **481**, 355 (2003).
[6] D. Funfschilling *et al.*, J. Fluid Mech. **536**, 145 (2005).
[7] G. Ahlers, F. Fontenele Araujo, D. Funfschilling, S. Grossmann, and D. Lohse, Phys. Rev. Lett. **98**, 054501 (2007).
[8] S. Grossmann and D. Lohse, Phys. Fluids **16**, 4462 (2004).
[9] E. S. C. Ching, H. Guo, X. D. Shang, P. Tong, and K. Q. Xia, Phys. Rev. Lett. **93**, 124501 (2004).
[10] D. Funfschilling and G. Ahlers, Phys. Rev. Lett. **92**, 194502 (2004).
[11] C. Resagk *et al.*, Phys. Fluids **18**, 095105 (2006).
[12] S.-L. Lui and K.-Q. Xia, Phys. Rev. E **57**, 5494 (1998).
[13] R. du Puits, C. Resagk, A. Tilgner, F. H. Busse, and A. Thess, J. Fluid Mech. **572**, 231 (2007).
[14] A. Maystrenko, C. Resagk, and A. Thess, Phys. Rev. E **75**, 066303 (2007).
[15] J. W. Deardorff and G. E. Willis, J. Fluid Mech. **28**, 675 (1967).
[16] D. E. Fitzjarrald, J. Fluid Mech. **73**, 693 (1976).
[17] A. Belmonte, A. Tilgner, and A. Libchaber, Phys. Rev. E **50**, 269 (1994).
[18] Y.-B. Xin, K.-Q. Xia, and P. Tong, Phys. Rev. Lett. **77**, 1266 (1996).
[19] X.-L. Qiu and K.-Q. Xia, Phys. Rev. E **58**, 5816 (1998).
[20] R. L. J. Fernandes and R. J. Adrian, Exp. Therm. Fluid Sci. **26**, 355 (2002).
[21] M. Ciofalo, M. Signorino, and M. Simiano, Exp. Fluids **34**, 156 (2003).
[22] C. Sun, Y.-H. Cheung, and K.-Q. Xia, J. Fluid Mech. **605**, 79 (2008).
[23] R. du Puits, C. Resagk, and A. Thess, Phys. Rev. Lett. **99**, 234504 (2007).
[24] E. Brown and G. Ahlers, J. Fluid Mech. **568**, 351 (2006).
[25] R. du Puits, C. Resagk, and A. Thess, Phys. Rev. E **75**, 016302 (2007).
[26] K.-Q. Xia, C. Sun, and S.-Q. Zhou, Phys. Rev. E **68**, 066303 (2003).
[27] R. Verzicco and R. Camussi, J. Fluid Mech. **383**, 55 (1999).
[28] K.-R. Sreenivasan, A. Bershadskii, and J.-J. Niemela, Phys. Rev. E **65**, 056306 (2002).
[29] H. Schlichting and K. Gersten, *Boundary Layer Theory*, 8th ed. (Springer, New York, 2004).
[30] R.-H. Kraichnan, Phys. Fluids **5**, 1374 (1962).
[31] S. Grossmann and D. Lohse, Phys. Rev. E **66**, 016305 (2002).
[32] X. Chavanne, F. Chillá, B. Chabaud, B. Castaing, and B. Hébral, Phys. Fluids **13**, 1300 (2001).
[33] D. Funfschilling, E. Bodenschatz, and G. Ahlers, Phys. Rev. Lett. **103**, 014503 (2009).
[34] J. H. Preston, J. Fluid Mech. **3**, 373 (1958).
[35] C. H. B. Priestley, Aust. J. Phys. **7**, 176 (1954).
[36] R. J. Adrian, R. T. D. S. Ferreira, and T. Boberg, Exp. Fluids **4**, 121 (1986).
[37] Y.-B. Xin and K.-Q. Xia, Phys. Rev. E **56**, 3010 (1997).
[38] J. J. Niemela and K. R. Sreenivasan, J. Fluid Mech. **557**, 411 (2006).